Electrochimica Acta 425 (2022) 140705

Contents lists available at ScienceDirect

Electrochimica Acta

journal homepage: www.journals.elsevier.com/electrochimica-acta

Mechanically and thermally robust microporous copolymer separators for lithium ion batteries

Alexander J. Manly [a], Wyatt E. Tenhaeff [a,b,*]

[a] Materials Science Program, University of Rochester, Rochester, NY 14627, United States
[b] Department of Chemical Engineering, University of Rochester, Rochester, NY 14627, Unites States

ARTICLE INFO

Keywords:
Separators
Polymerization induced phase separation
Co-polymer
Batteries

ABSTRACT

Next generation, multifunctional separators can enhance energy storage, power, and safety performance of lithium ion batteries but must be simple to fabricate and incorporate with existing roll-to-roll manufacturing. This study presents a strategy to facilely prepare these separators using UV-initiated polymerization-induced phase separation (PIPS), wherein microporous polymer separators are fabricated directly from constituent monomers and ethylene carbonate (EC) porogen. This enables a wide compositional design space as co-monomers with specific chemical functionality can be readily incorporated into the PIPS precursor mixture. Herein, 1,4-butanediol diacrylate (BDDA) was copolymerized with poly(ethylene glycol) diacrylate (PEGDA) to increase the acrylate conversion in the photopolymerization and improve mechanical properties. By tuning the ratio of PEGDA and EC, separators with high porosity (41.3%) and effective ionic conductivity (2.09 mS cm^{-1}) were prepared. Inclusion of PEGDA was essential to increasing the elastic modulus to > 345 MPa, which is required for cell assembly by roll-to-roll manufacturing. All separators prepared were shown to enable reversible cycling of lithium metal/$LiNi_{0.5}Mn_{0.3}Co_{0.2}O_2$ half-cells for 100 cycles. Unlike conventional polyolefin separators, which were shown to melt at 160 °C and shrink by up to 29.8% at elevated temperatures, the PIPS separators possess exceptional, safety-enhancing thermomechanical properties, undergoing no phase transitions or thermal shrinkage.

1. Introduction

Electrochemical energy storage in the form of lithium ion batteries (LIBs) is essential to modern daily life, powering portable consumer electronics and electric vehicles. Over the past decade significant material advances in electrode active materials (both anode and cathode) have significantly improved cell-level energy densities, while the economies of scale of massive LIB manufacturing facilities have reduced battery costs [1,2]. Increasingly, these low cost, energy-dense LIBs are enabling novel applications and devices. Yet, because conventional LIBs rely on flammable aprotic liquid electrolytes, safety remains a serious concern [3,4].

Separators are critical to LIB cell performance and safety. Their primary role is to physically isolate the anode and cathode without significantly impeding ion transport in the liquid electrolyte. Several excellent resources describe the key material properties that separators should possess to enable safe, long-term operation of LIB cells [5–8]. State-of-the-art LIB separators are microporous polyolefin materials, composed of polyethylene (PE) and/or polypropylene (PP), with a porosity of approximately 40% (v/v). While these separators have served admirably in LIBs, there are notable opportunities to improve upon them [9]. The hydrophobicity of these materials leads to relatively poor electrolyte uptake and lackluster effective ionic conductivity, despite their high porosity [7,10,11]. Polyolefin separators also suffer from severe thermal shrinkage at elevated temperatures, which can lead to electrode contact and short circuiting, causing cell failure and thermal runaway [4,12]. This failure mechanism is one of the primary causes of fire safety hazards in LIBs [13]. Although the melting of polyethylene (circa 135 °C) in laminated PP/PE/PP trilayer separators is designed as a thermal fuse safety mechanism, there is evidence that the increase in impedance resulting from the melting of the polyolefin layers is insufficient to fully halt thermal runaway processes in high-voltage applications such as battery electric vehicles and stationary storage [14,15]. Thus, the temperature inside such a cell can continue to rise, and at temperatures above 165°C the polypropylene component will also melt, increasing the probability of inter-electrode contact [14,16].

* Corresponding author.
E-mail address: wyatt.tenhaeff@rochester.edu (W.E. Tenhaeff).

https://doi.org/10.1016/j.electacta.2022.140705
Received 11 May 2022; Received in revised form 2 June 2022; Accepted 11 June 2022
Available online 12 June 2022

Furthermore, a polyolefin separator is at risk of melting and short-circuiting when exposed to an external heating source, leading to the propagation of catastrophic cell failure should a multi-cell battery pack become compromised [16].

Considerable effort has been directed towards addressing these safety and performance challenges in polyolefin separators [17–20]. Surface chemistry modification of polyolefins to enhance electrolyte wettability/compatibility through various coating/grafting methods and application of a layer of ceramic particles to improve impact resistance and mitigate thermal shrinkage are common strategies to improve separator performance [21–23]. Other approaches include designing organic-inorganic composites [4,24–27] and formulating the separators with thermally stable polymers, often possessing stiff aromatic backbones, [16,28,29] to enhance thermochemical stability. However, these material fabrication approaches are fairly complex, requiring additional processing steps, and they utilize less common, lower-volume chemical precursors. Moreover, the ceramic coating layers and inorganic composites increase the separator mass and/or volume, ultimately compromising the effective specific energy and energy density of the overall cell.

It is essential that simple, low-cost, scalable fabrication methods be developed for separators that address the limitations of existing separators without compromising safety, performance, or manufacturing [30–32]. Moreover, these methods should enable next-generation multifunctional separators, which are membranes that in addition to possessing the requisite chemical, thermal and physical properties, also play an active role in mitigating undesirable side reactions in the cell and enhance reversibility and stability of the electrochemical cells. Examples of this multifunctionality are the inclusion of acid and transition metal cation scavenging moieties [33–39], incorporation of polysulfide barriers and electrostatic screening in Li-S batteries [40–45], and the development of structural separators with optimized mechanical properties to reinforce an electrochemical cell that is both an energy storage device and structural member [46,47]. These separators promise to maximize the value of a separator and improve the safety and energy storage performance of the cells [13].

A facile one-step synthesis method to precisely design microporous separators was previously introduced. By exploiting ethylene carbonate (EC), which is an indispensable component of LIB electrolytes, and polymerization-induced phase separation (PIPS), microporous polymers can be rapidly fabricated through UV photopolymerization [48]. UV photopolymerization is a low-cost, high throughput method that has been extensively explored for lithium ion battery manufacturing [49,50]. As the unsaturated monomers polymerize and crosslink, the EC phase separates into nanoscale domains, forming pores. But because EC is an electrolyte component, further extraction and separator purification is not required [48]. High porosity and ionic conductivity were achieved through this strategy, and the separators demonstrated performance comparable to state-of-the-art polyolefin separators. It was also shown that these separators exhibit excellent thermomechanical stability due the high crosslinking density of the thermoset network. However, the mechanical properties of the high-performance separators were inadequate for roll-to-roll LIB assembly. It was suggested that separator properties could be further tuned through copolymerization, demonstrating opportunities to engineer multifunctionality through the PIPS method. In this study, the co-monomer poly(ethylene glycol) diacrylate (PEGDA) was incorporated into a precursor solution, where 1,4-butanediol diacrylate (BDDA) is the major component. PEGDA was selected as it is expected to increase the elastic modulus and strength of the coating, [51] and for the well-established kinetic stability of polyethylene glycol (PEG) in LIB systems [52–54]. The incorporation of a minor amount of PEGDA strongly influenced the polymer mechanical properties, as well as the separator morphology, demonstrating the ability to tune separator properties in this scalable, one-step process. An optimized formulation was then developed which yielded a microporous separator with 41.3% porosity, ionic conductivity of 2.09 ± 0.28 mS cm^{-1}, and sufficient elastic modulus ($\geq$ 345 MPa) for feasibility with current LIB cell assembly methods.

2. Experimental

2.1. Materials and separator fabrication

All chemical reagents and components were used as-received from the manufacturer. Technical grade 1,4-butanediol diacrylate (BDDA, $\geq$87% purity) and anhydrous ethylene carbonate (EC, 99% purity) were purchased from Sigma-Aldrich. Poly(ethylene glycol) diacrylate (PEGDA), molecular weight = 400 g mol^{-1}, n ~ 9, was purchased from Scientific Polymer Products Inc. 2-benzyl-2-(dimethylamino)-4'-morpholino butryophenone (Omnirad 369) was a gift from IGM Resins. Standard conductivity solutions made of aqueous KCl were purchased from Fisher Scientific. $LiNi_{0.5}Mn_{0.3}Co_{0.2}O_2$ (NMC532) positive electrode used in this experiment were produced at the U.S. Department of Energy's (DOE) CAMP (Cell Analysis, Modeling and Prototyping) Facility, Argonne National Laboratory. The cathode material was 90 wt% NMC532, 5 wt% Timcal C45 (conductive additive), and 5% Solvay 5130 PVDF binder. The coating thickness was 34 μm and the areal loading density was 9.12 mg cm^2. The battery electrolyte was 1M $LiPF_6$ in 3:7 v/v ethylene carbonate/dimethyl carbonate, purchased from MTI Corporation. Celgard 2500 was a gift from Celgard. All chemicals were used as-received without further purification.

PIPS precursor solutions were prepared by mixing BDDA and PEGDA in the appropriate ratios. The solutions and resulting polymers were designated by the mass percent of the monomer mixture made up by PEGDA. EC was added to the monomer mixture, and the whole mixture was slowly heated to around 33 °C until the EC melted and formed a homogenous solution with the monomer. Upon cooling to room temperature, the EC remained in solution. Omnirad 369 initiator was then added to the mixture to a ratio of 0.1% w/w and was sonicated for 30 s.

Three drops of the precursor solution were placed on a 2"x3" glass slide. A second glass slide was set on top of the solution to spread it out. This method resulted in films of 20–25 μm in thickness. Thicker films were obtained using 50 μm-thick pressure adhesive tape as spacers. The slides were then placed under a long-wave UV lamp (20 mW cm^{-2}) for 10 min, flipping the slides halfway through the cure.

After the cure, the slides were carefully separated using a razor blade. For removal of the porogen, the solid polymer film was placed in an acetone bath. The films were rinsed with fresh acetone three times to remove any residual EC and dried on a clean aluminum pan at 70 °C overnight. The films could then be cut or punched into whatever size or shape was necessary, their thicknesses were then verified using a digital micrometer (Pittsburgh).

2.2. Compositional and physical characterization

2.2.1. Fourier transform infrared spectroscopy (FTIR)

IR absorption spectra were obtained for non-porous polymer films using monomer ratios identical to those used for separator fabrication. Samples were prepared the same as above, but without the inclusion of the porogen. Spectra were obtained on a Nicolet iS50 FT-IR using a single reflection Specac Golden Gate attenuated total reflectance (ATR) attachment. Thirty-two spectra were integrated at a resolution of 4 cm^{-1}. Absorbance data was normalized to the acrylate carbonyl peak for analysis.

2.2.2. Electrolyte uptake

The mass of dry separators was first measured. They were then soaked in battery electrolyte. The wet samples were dabbed to remove excess electrolyte on the surface. Once the mass of the soaked sample was equilibrated, it was recorded. This measurement was repeated with four separate samples for each material, and the averages were reported.

2.2.3. Thermal analysis

Thermal stability of samples was tested on a TA Instruments Discovery TGA under a nitrogen purge flow of 25 mL min^{-1}, from 50 to 700 °C with a ramp rate of 5 °C/min.

DSC was performed on a TA Instruments DSC Q2000, using TZero aluminum pans and hermetic lids. Under a nitrogen purge of 50 mL min^{-1}, samples were ramped at 10 °C/min from 0 to 200 °C four times to ensure repeatability.

To measure thermal shrinkage, separators were prepared using above methods and punched into a circular shape with diameter of 0.75 in. Celgard 2500 samples were also punched into a circular shape of equal area. A digital image of each separator material was taken in front of a piece of paper with a known 5in x 5in area at room temperature after equilibrating at elevated temperature for 30 min. Computer vision analysis was used to compute the area of the separator materials for each image, enabling the quantitative comparison of separator areas before and after heating.

2.2.4. Scanning electron microscopy (SEM)

Separator morphology was characterized using a Zeiss Auriga SEM/FIB at an accelerating voltage of 3 kV. Prior to observation, all EC was removed from the samples as described above, which were then sputter coated with gold on a Denton Vacuum DESK-II DC sputtering system. Samples were sputter coated for 60 s, leading to a coating of about 70 Å. From the SEM micrographs, porosity estimates were obtained with a computer vision algorithm which detects the fraction of area occupied by pores in the sample image, using brightness thresholding and contour detection methods from the openCV Python library [55].

2.2.5. Mechanical testing

Stress-strain curves were obtained using a TA Instruments RSA-G2 solids analyzer. Samples were cut to a 6 × 12 mm rectangle, and their thickness was measured using a digital micrometer to determine cross-sectional area. Samples were clamped on each end with an initial gap of 5 mm. Samples were equilibrated to 25 °C, and a strain sweep was performed at a strain rate of 0.67% s^{-1}. Elastic moduli were determined through linear regression of the stress-strain data up to a strain of 1.5%.

2.2.6. Contact angle measurements

Static water contact angles (WCAs) were obtained using a Biolin Scientific Theta Lite Tensiometer. Samples were laid flat on the bed, and a digital video was recorded as a single drop of was dispensed on the surface. A frame was chosen after the contact angle equilibrated.

2.3. Electrochemical characterization

2.3.1. Electrochemical impedance spectroscopy (EIS)

The ionic conductivities were determined using AC impedance spectroscopy. Polymer films were tested using a Swagelok T-cell (pictured in Fig. S1), where the film is held between two blocking stainless steel electrodes with a diameter of 3/8". The inner cavity was then filled with battery electrolyte, ensuring full uptake, and the openings were tightly capped. These T-cells were assembled inside an argon-filled glovebox, but then removed for testing. The cells were placed inside a Tenney Jr. environmental chamber and connected to a Solartron SI 1260 impedance analyzer using a two-electrode setup. Before each measurement, the cell was equilibrated to the desired temperature for 45 min. Sweeps were performed from a frequency of 1 MHz to 0.1 Hz, with an AC amplitude of 10 mV. The ionic resistances were simply taken to be the real impedance intercept on the resulting Nyquist plot. To account for ohmic and contact resistances introduced by the Swagelok T-cells and increase confidence in reported ionic conductivities, each material was measured with three different thicknesses. For Celgard 2500, membranes were layered to vary the thickness. The resistivity of each material was then obtained by taking the slope of area-specific resistance (ohm•cm^2) versus thickness.

The ionic conductivity of the battery electrolyte was measured using an Accument 2-cell conductivity probe connected to the same Solartron impedance analyzer inside an environmental chamber. This probe was first calibrated using a series of standard KCl solutions (447 μS cm^{-1}, 1000 μS cm^{-1}, 8974 μS $cm^{-1}$and 15,000 μS cm^{-1}).

2.3.2. Construction of electrochemical half cells

In order to test the separators, electrochemical half-cells were constructed using a CR2032 coin cell format, entirely in an argon-filled glovebox. The half-cell format was used to eliminate as many variables as possible. The negative electrode was fabricated by first cutting off a piece of lithium ribbon, and scraping off the oxide layer with a wire brush. The lithium was then rolled flat with a piece of PVC tubing and punched to a diameter of 5/8 in using a hollow punch. These operations were performed on top of a clean polypropylene sheet. A piece of positive electrode material was cut off using scissors, placed inside a folded piece of weighing paper, and electrodes were punched out to a diameter of 1/2 in using a paper punch.

The cell was constructed in the following order: the negative electrode cap was placed down, a wave spring placed inside, and a stainless-steel spacer placed on top of that. The lithium electrode was then centered on the spacer. Battery electrolyte was dropped onto the lithium, and the separator was placed on this electrolyte to allow wetting. Electrolyte was dropped on the positive electrode to allow wetting of the porous active material, and then set on top of the separator, being sure to center the positive electrode with the lithium, ensuring full overlap. The positive electrode cap was then pressed onto the negative electrode cap, and the full construction was crimped in a MTI MSK-160D electric crimper. The coin cells were then removed from the glovebox, wiped down with acetone, and labelled.

2.3.3. Electrochemical cycling

Cells were cycled at 30 °C using a Neware battery testing system. Cycling procedures were adapted from Argonne National Lab's published protocols for testing LIBs [56]. The first step of all cycling was a formation step. This consisted of first applying a tap charge of 1.5 V for 15 min. The cells were then rested for 6 h to allow for full electrolyte wetting and equilibration. The cells were then cycled twice at a C/10 rate. The long-term performance of cells was tested by cycling the cells at C/3 for 100 cycles between 3 V and 4.2 V or between 3 V and 4.4 V. The charging steps used a C/20 cut-off current while the discharge steps simply cut-off at 3 V.

3. Results and discussion

In this study, several copolymer networks of varying compositions were prepared as LIB separators. They were labelled according to corresponding PIPS precursor solution compositions. The difunctional monomer 1,4-butanediol diacrylate (BDDA) was the main multifunctional component in the polymer composition, and poly(ethylene glycol) diacrylate (PEGDA) was included as a minor co-monomer. For all PIPS precursor solutions, ethylene carbonate (EC) was used as the porogen. BDDA was chosen as a major component in these formulations because it was recently shown that a PIPS precursor mixture of BDDA and EC undergo UV-initiated PIPS, resulting in a microporous morphology, high thermomechanical stability, and stable cycling when incorporated into a LIB half-cell [48]. PEGDA was chosen as a minor additive in order to improve the polymerization kinetics of the PIPS mixture and for its well-known kinetic stability in LIBs [52–54]. The microporous separators were labelled as *XX*PEG-*YY*EC, where *XX* refers to the mass percent of the co-monomer mixture that was the PEGDA (the balance was BDDA), and *YY* refers to the mass percent of EC in the total PIPS solution. For example, 5PEG-60EC was 60% w/w EC, 2% w/w PEGDA and 38% w/w BDDA. The mixture was 2% w/w PEGDA because it was 5% of the total monomer weight in the precursor solution (40% w/w). In many cases, these PIPS separators were compared to a commercial

polypropylene (PP) separator, Celgard 2500.

Fourier transform infrared spectroscopy was first used to confirm the chemical composition of the cured polymer networks. Fig. 1a provides the FTIR spectra of the monomer precursors. Characteristic of BDDA and PEGDA, which are both acrylates, a strong vibrational mode at 1723 cm^{-1}, assigned to the carbonyl stretch, and two weak absorbances at 1615 cm^{-1} and 1645 cm^{-1}, corresponding to C=C stretch modes, are observed in the monomer precursors [57]. After UV-initiated radical polymerization, the carbonyl functionalities remain unchanged, while the vinyl groups are converted to an aliphatic polymer backbone. This is demonstrated in Fig. 1b, showing the FTIR spectra for all of the polymers. All samples exhibit an unchanged carbonyl stretch, whereas the absorbances of the vinyl stretching modes are reduced. The polymerization solution undergoes a physical transformation from liquid to a solid, which is insoluble in organic solvent, suggesting the formation of a crosslinked polymer network.

For analysis, all FTIR data was normalized to the maximum absorbance of the carbonyl stretching peak at 1723 cm^{-1}. It was expected that a crosslinked copolymer can be prepared by photopolymerizing a homogenous solution of acrylate co-monomers. Fig. 1c,d clearly demonstrates the ability to control the chemical compositions of the polymers through the relative concentrations of co-monomers in solution. The spectra in Fig. 1a shows that PEGDA exhibits a medium-strength peak at 2873 cm^{-1} from the C-H stretches of the CH_2 groups in the poly(ethylene glycol) backbone of the macromer [58]. BDDA possess this peak, but it is much weaker given its fewer methylene groups. Furthermore, these functionalities are not altered by the polymerization process, and these functionalities will persist in the cured copolymer network. Fig. 1c shows that not only is the CH_2 stretch present in the polymer spectrum, but its absorbance is correlated to the PEGDA concentration. This indicates that PEGDA concentration is effectively being modulated within the polymer network. Similarly, the PEGDA spectrum has a peak at 1115 cm^{-1} corresponding to the stretching of the ether bonds in the poly (ethylene glycol) backbone. BDDA exhibits no such peak. Again, the absorbance of this vibrational mode is correlated to the PEGDA concentration in the precursor solutions, as shown in Fig. 1d. These trends in the infrared absorbances indicate that PEG functionality was successfully incorporated into the final copolymer, and that it was possible to control the PEG fraction of the copolymer through the precursor solution formulation.

Upon close inspection of the vinyl stretching range from 1615 to 1645 cm^{-1}, it was found that PEGDA content had an effect on monomer conversion during the UV polymerization step. These peaks are a direct observation of the extent to which the acrylate functionalities were converted. The data in Fig. 1e clearly shows that the 0PEG sample had the lowest acrylate conversion, followed by 5PEG, 7PEG, 15PEG, and 30PEG. This trend is also observed in the wagging mode of the acrylate CH_2 group at 810 cm^{-1}. An obvious trend of decreasing absorbance of this peak with increasing PEG content is shown in Fig. 1f. This vibrational mode is popularly used to observe acrylate conversion as it is a sharp, single peak, with strong absorption compared to the vinyl stretching modes [59,60]. This further indicates an increase in monomer conversion of the high-PEGDA formulations. This phenomenon is explained by the increased mobility of acrylate functional groups afforded by PEGDA pendant groups during polymerization. During propagation, one reactive acrylate group may be incorporated into the polymer network, leaving the second unreacted pendant vinyl immobilized. Since BDDA is a shorter monomer, the radius in which another

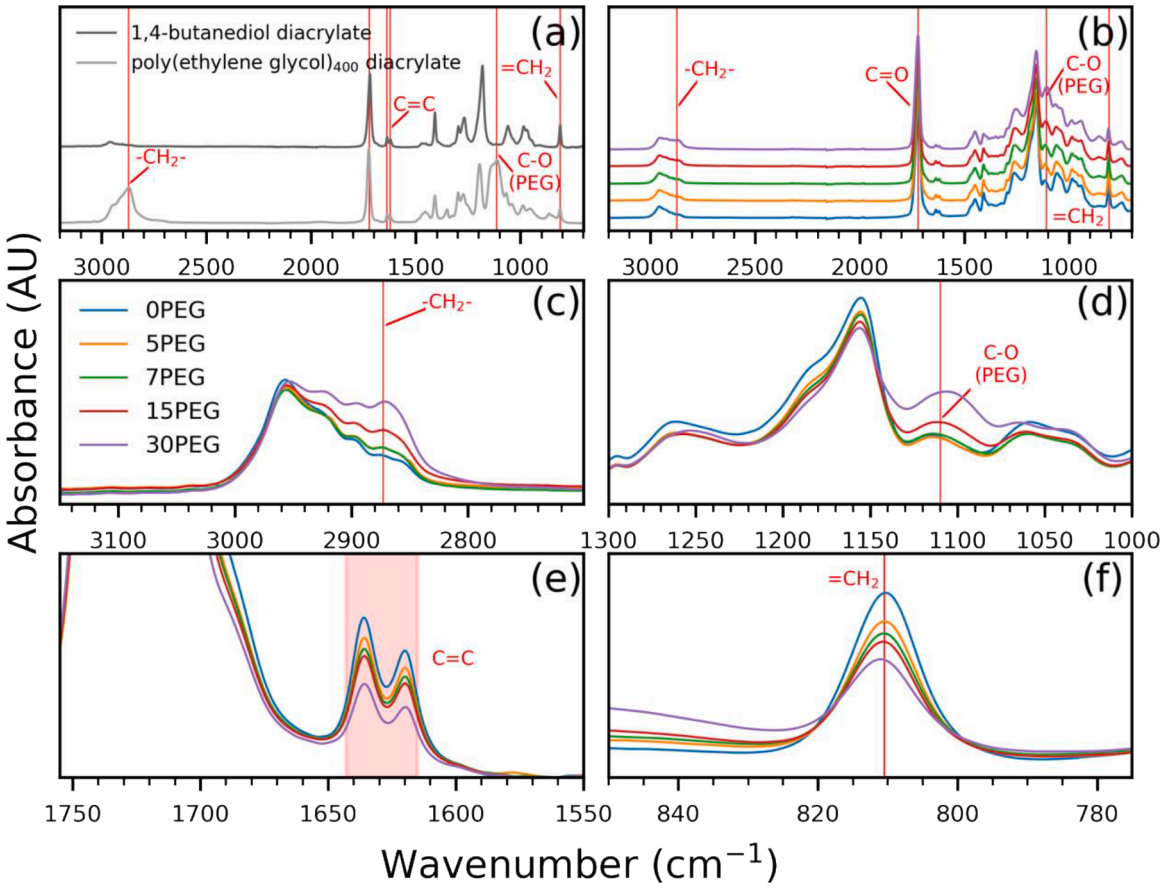

Fig. 1. FTIR-ATR spectra, normalized to the C=O stretching mode at 1723 cm^{-1} showing (a) precursor diacrylate monomers, (b) UV-curved and acetone-washed polymer films, and magnification of the spectra in (c) the C-H stretching range 2700–3150 cm^{-1}, (d) the ester and ether stretching range 1050–1250 cm^{-1}, (e) the vinyl stretching range 1550–1750 cm^{-1}, and (f) the vinyl CH_2 wagging mode at 810 cm^{-1}.

activated acrylate must come within to form a cross-link is small, lowering the probability that the acrylate group will be converted. By incorporating a long-chain monomer like PEGDA, the radius over which the unreacted acrylate pendant may search to find a propagating chain is much larger. Thus, a greater proportion of acrylate functional groups will be converted and form cross-links [61].

Static water contact angles (WCAs) were measured for each separator composition. These results are included in Table 1. The WCAs are a function of both the hydrophilicity of the polymer chemistry and porosity. Hydrophilic polymers will result in lower WCAs, while materials with larger pores will also lead to lower WCAs due to exhibiting more Wenzel than Cassie-Baxter state character [62]. Despite the multivariate relationship between the materials and their WCAs, the WCAs of the separators generally decreased with average pore size. Furthermore, WCAs increased with the PEGDA content because the PEG moieties are less polar than the acrylates, which are diluted by the incorporation of PEGDA. Most importantly, all PIPS separators exhibited a greater hydrophilicity than Celgard 2500, which provides for better uptake and wetting of the highly polar aprotic LIB electrolytes.

By changing the kinetics of polymerization and phase separation, the incorporation of PEGDA into the precursor solution altered the pore morphology of the porous separators. This is apparent from the SEM images of the separators in Fig. 2 for various PEGDA concentrations. The insets in Fig. 2 are digital photographs of the polymer samples obtained after removing the porogen, revealing the translucent/opaque appearance of the separators due to the scattering of light by the porous morphology. For a fixed EC concentration, the opaqueness decreased as the concentration of PEGDA increased, suggesting that the porosity and/or pore size is inversely correlated to PEGDA content. This is also observed qualitatively in the SEM micrographs in panels 2a–d.

Table 1 provides the porosity and average pore size of these samples quantified from the SEM images using a computer vision algorithm, which confirms the trend in reduced porosity and pore sizes. The contours detected by the algorithm have been overlaid on top of the original SEM images and included in Fig. S2. The effect of PEGDA on porous domain size can explained by the high viscosity of the PEGDA component, which increases the overall viscosity of the reaction solution. Studies have shown the incorporation of high viscosity additives into PIPS solutions generally results in reduced phase domain sizes [63,64]. This is due to the lower diffusion rates, slowing the evolution of spinodal decomposition and arresting phase separation before large domain sizes can evolve [65,66]. Faster polymerization kinetics will lead to network formation, also arresting phase separation. The pore size distribution is plotted in a histogram in Fig. S3 for each porous sample studies. These distributions illustrate that increased PEGDA content during polymerization led to a more homogeneous morphology with a greater frequency of small domain sizes. A reduction in porosity was also observed with high PEGDA concentration. This is presumably due a slight miscibility of EC with PEG, which allows EC to associate with the PEG-400 chains in the PEGDA forming a gel-like phase [67]. During the PIPS process, some of the EC can remain in the polymer matrix, effectively reducing the amount of porogen that phase separates and reducing the porosity. Thus, as the PEG content increases in the polymer formulation with higher PEGDA concentrations, the capacity for EC in the cured polymer matrix increases and the porosity will decrease.

The effect of PEGDA on polymer film strength was investigated through mechanical measurements of the dense polymer material devoid of pores. The dense copolymer films were examined to decouple the effect of PEGDA from polymer porosity. Uniaxial tensile stress-strain curves are presented in in Fig. 3a. It was observed that the introduction of PEGDA initially increased the modulus of the polymer, but at a PEGDA concentration of 15% (w/w), the higher PEG content in the polymer results in the film decreasing in modulus and becoming more elastic. The initial increase in modulus of the polymer film is attributed to higher monomer conversion associated with PEGDA, which was demonstrated above. However, the mechanical improvement through higher conversion was eventually offset by the inherent compliance of the PEG chains as the PEGDA content was increased.

Stress-strain curves of the porous materials were also collected, shown in Fig. 3b, and the elastic moduli are reported in Table 1. These results revealed a complex relationship with PEGDA content, owing to the decreased porosity and changes in modulus with increasing PEG content. The modulus of 5PEG-60EC was significantly greater than 0PEG-60EC, which is a function of both the increased modulus of the bulk polymer and lower porosity. Polymer film modulus again increased with 15PEG-60EC, despite the lower modulus of the dense polymer, due to a large drop in porosity from the 5PEG-60EC sample. The porosity of 30PEG-60EC was the lowest measured, but because of the inherent compliance of the high concentration of PEGDA, this porous film was slightly more compliant than 15PEG-60EC.

In the context of LIB separators, modulus is pertinent when considering LIB assembly. Full cells are assembled by the unwinding of electrode and separator rolls, and stacking through a roll-to-roll process. During this process, the sheets of material are put under uniaxial tension. The industry standard requires that separator material undergo less than 2% strain at 1000 psi of strain [5]. This requirement is illustrated in the inset of Fig. 3b. The horizontal grey line represents a range of moduli a separator material should possess for feasibility in a roll-to-roll process. The stress-strain curves that pass through the horizontal grey line meet the requirements for roll-to-roll assembly, and the curves that pass through the black line do not. Most of the samples with 60% EC did not exhibit both high porosity and sufficient modulus. 5PEG-60EC just barely passes the modulus requirement. It was then hypothesized that by optimizing PEGDA and EC concentrations in the PIPS precursor solution, it is possible to simultaneously increase polymer modulus to satisfy the roll-to-roll manufacturing requirements while increasing porosity, which will benefit ion transport (conductivity). The formula of 7PEG-63EC was identified for this purpose. This formulation provided the highest porosity (41.3%), while the elastic modulus exceeds the requirement for roll-to-roll assembly, as seen in this inset of Fig. 3b. The maximum stress of the 7PEG-63EC film was somewhat low due to the higher porosity of the material, but battery separators typically do no undergo this amount of strain. Thus, this polymer was considered an optimized LIB separator material for existing processes.

To evaluate the electrochemical transport properties of the PIPS separators, the ionic conductivity of each material was measured. This

Table 1
Physical properties of the LIB separators fabricated by PIPS.

Sample	Porosity (%)	Avg. pore radius (nm)	Uptake (%)	σ_{eff} (mS cm^{-1})	N_M	E_A (kJ mol^{-1})	WCA (°)	Modulus (MPa)
0PEG-60EC	38.5	22.0	127 ± 14	1.98 ± 0.08	4.8	13.4 ± 1.6	33.8	272
5PEG-60EC	37.4	14.0	129 ± 15	1.59 ± 0.05	6.0	12.9 ± ± 0.8	53.0	373
15PEG-60EC	27.7	10.9	106 ± 5	1.33 ± 0.36	7.1	14.9 ± 3.4	64.6	542
30PEG-60EC	20.6	7.6	99 ± 12	1.01 ± 0.06	9.4	18.1 ± 1.0	49.9	504
7PEG-63EC	41.3	19.6	108 ± 7	2.09 ± 0.28	4.5	12.7 ± 1.8	61.8	450
Celgard 2500	55.0[‡]	32.0[‡]	98 ± 5	1.62 ± 0.13	5.1	13.4 ± 1.1	87.5	729(MD), 273(TD)

[‡] Values reported by manufacturer. σ_{eff} effective ionic conductivity. N_M MacMullin number. E_A activation energy. WCA water contact angle.

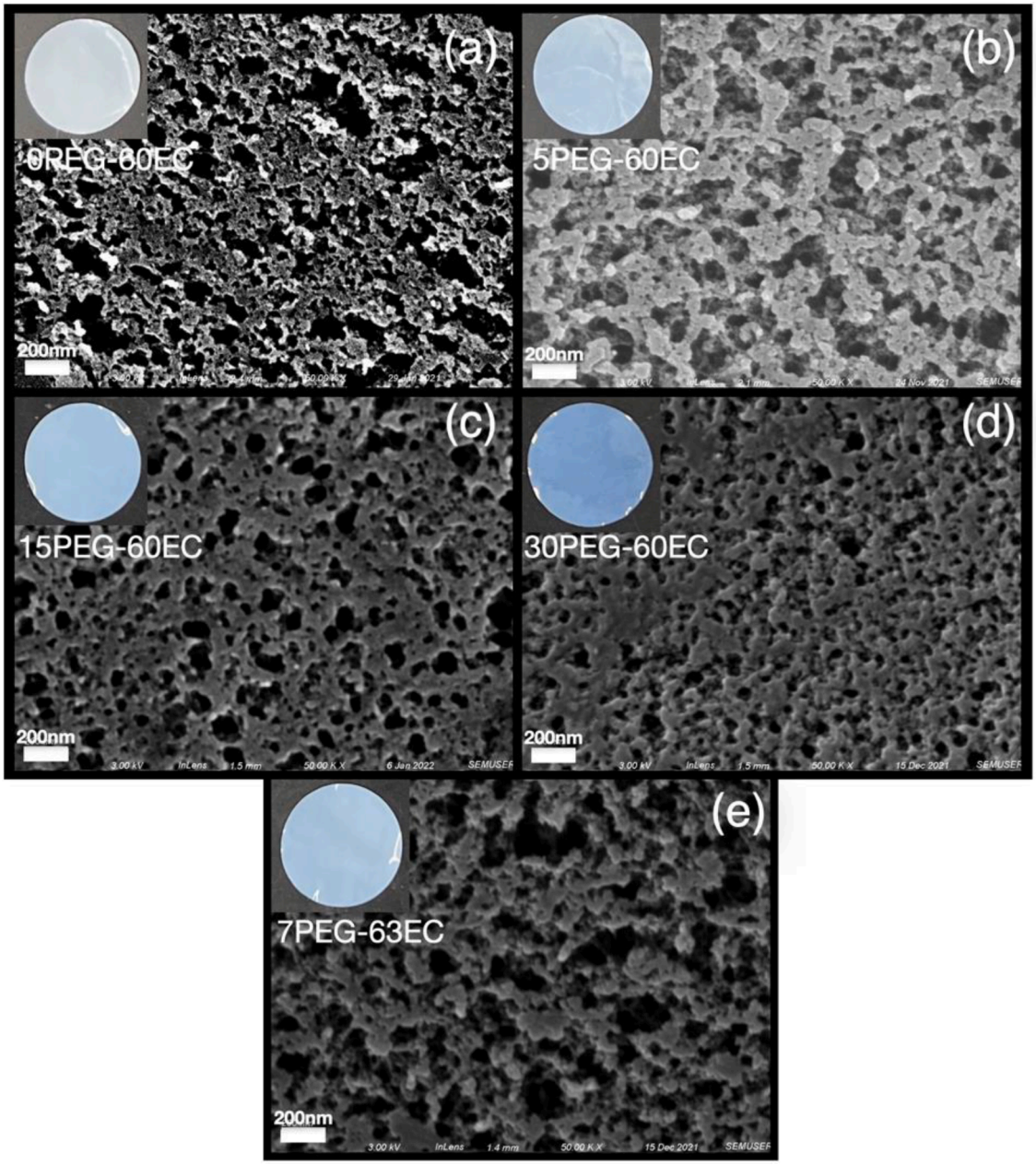

Fig. 2. SEM images of the porous polymers at 50,000X magnification: (a) 0PEG-60EC, (b) 5PEG-60EC, (c)15PEG-60EC, (d) 30PEG-60EC, and (e) 7PEG-63EC. Insets show digital images of the porous separators on a black background.

was conducted using a Swagelok-type T-cell. This setup, pictured in Fig. S1, held a sample of porous polymer between two stainless steel blocking electrodes. One of these blocking electrodes was attached to a spring, allowing for a standardized amount of pressure to be applied to the separator. A T-cell setup was used so that the cavity could be filled with electrolyte and sealed, so that the cell could be removed from the glovebox atmosphere and maximum electrolyte uptake was achieved. AC impedance testing was then performed in a temperature-controlled chamber. For each material formula, three or more samples were tested with different thicknesses to allow for the accurate subtraction of contact and ohmic resistances introduced by the Swagelok cells. Furthermore, experimental errors were minimized by taking multiple measurements and analyzing through regression.

An Arrhenius plot with data from the various porous polymers measured is displayed in Fig. 4. The corresponding effective ionic conductivities at 25 °C and activation energies are listed in Table 1. As expected, ionic conductivity roughly tracked with the measured porosity of the samples. However, the low-porosity samples were found to have better conductivities than might be expected for the given porosities. In particular, the 30PEG-60EC sample was only 20.6% porous, while the ionic conductivity was measured as 1.01 ± 0.06 mS cm^{-1}. This is likely explained by ionic conduction through liquid absorbed into the polymeric phase of the separator. Poly(ethylene) glycol is a well-known solid lithium ion conductor, and PEGDA-based formulations have been used extensively as polymer gel electrolytes [52,67–71]. 30PEG-EC is expected to have a significant amount of PEG chains, which form a gel phase with the electrolyte, allowing for lithium ion conduction between polymer chains. As seen in Table 1, this is supported by a relatively small drop in electrolyte uptake from 129% in 0PEG-60EC to 99% in 30PEG-60EC. This suggests that while the porosity was relatively low in the high-PEG samples, this effect was partially offset by electrolyte being absorbed in the polymeric framework of the separator. Partial

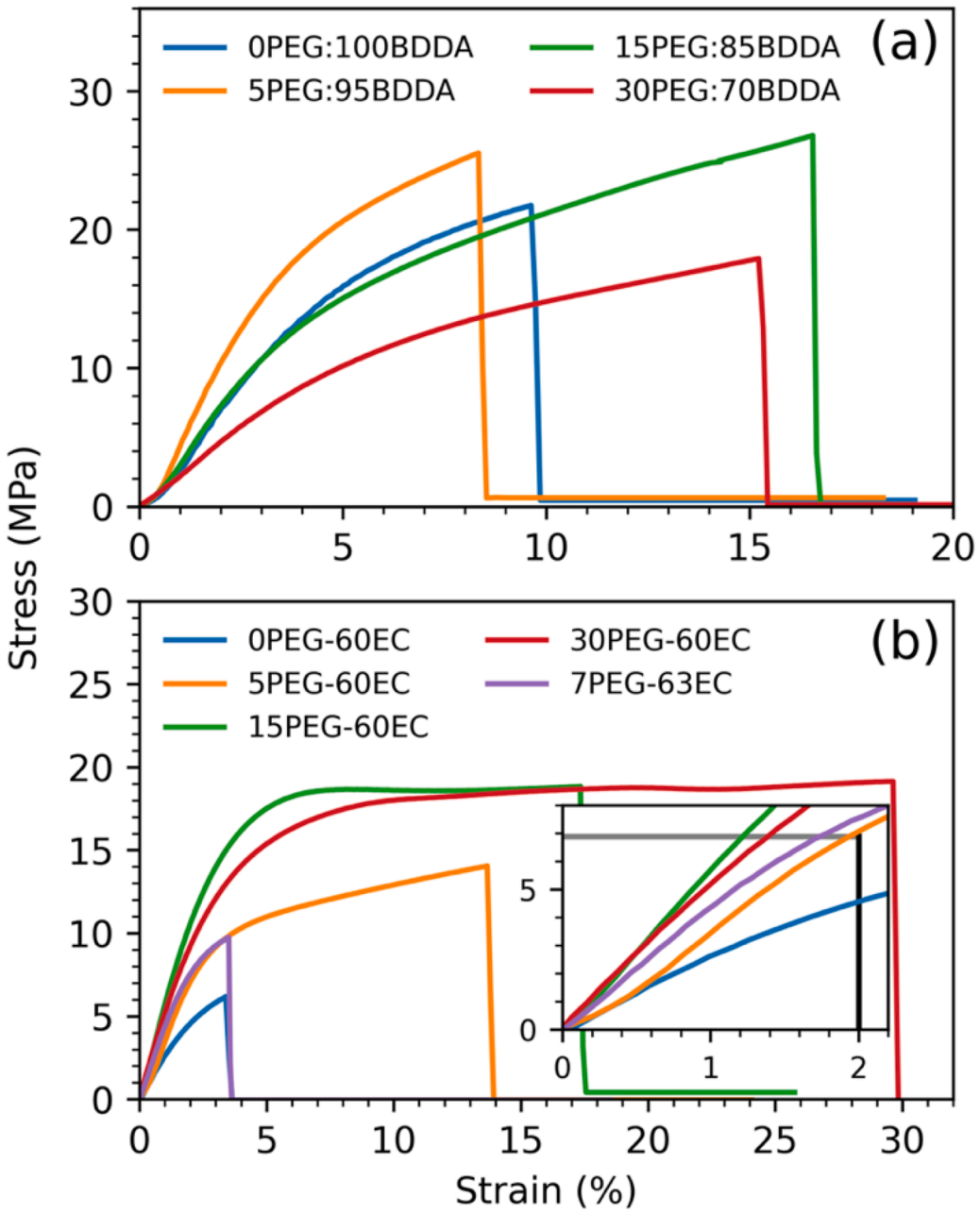

Fig. 3. Stress-strain curves of (a) non-porous polymer films and (b) corresponding porous films, including optimized separator. The inset illustrates the industry standard for roll-to-roll processing; curves that intersect the horizontal grey line meet the requirments, while curves that intersect the black line do not.

conduction through the gel phases is also supported by the measured increase in activation energy. Compared to pure electrolyte (activation energy of 13.8 ± 0.3 kJ mol^{-1}), the high-PEG samples, 15PEG-60EC and 30PEG-60EC, have slightly larger activation energies (14.9 ± 3.4 kJ mol^{-1} and 18.1 ± 1.0 kJ mol^{-1}, respectively), which is consistent with ionic conduction through a polymer gel phase [72]. Meanwhile, the activation energy for ionic conduction through 0PEG-60EC (13.4 ± 1.6 kJ mol^{-1}) and 5PEG-60EC (12.9 ± 0.8 kJ mol^{-1}) remained nearly identical to pure electrolyte, indicating conduction solely through liquid electrolytes phase (within the pores).

Ionic conductivity testing of 7PEG-63EC revealed that the aim of optimizing both mechanical properties and ionic conductivity was realized. Not only did this material satisfy modulus requirements, it was shown to possess the highest ionic conductivity at room temperature, 2.09 ± 0.28 mS cm^{-1}. This was expected given the superior porosity. It is an improvement over 0PEG-60EC, which was previously the most porous formulation with an effective ionic conductivity of 1.98 ± 0.08 mS cm^{-1} at 25 °C but did not satisfy modulus requirements. The optimized material also had a low activation energy of 12.7 ± 1.8 kJ mol^{-1}, suggesting that ionic transport also occurs exclusively through the electrolyte-filled porous phase.

A useful metric for comparing ionic conductivities among various separator materials is the MacMullin number, which is defined as:

$$N_M = \frac{\sigma_0}{\sigma_{eff}} \quad (1)$$

where N_M is the MacMullin number, σ_{eff} is the effective ionic conductivity of the electrolyte-saturated separator, and σ_0 is the ionic conductivity of the electrolyte [73,74]. N_M is useful because it controls for the composition of battery electrolyte employed in the study, the conductivity of which will depend on the exact formulation (salt concentration and solvent) [73]. Instead, N_M captures the effect of separator

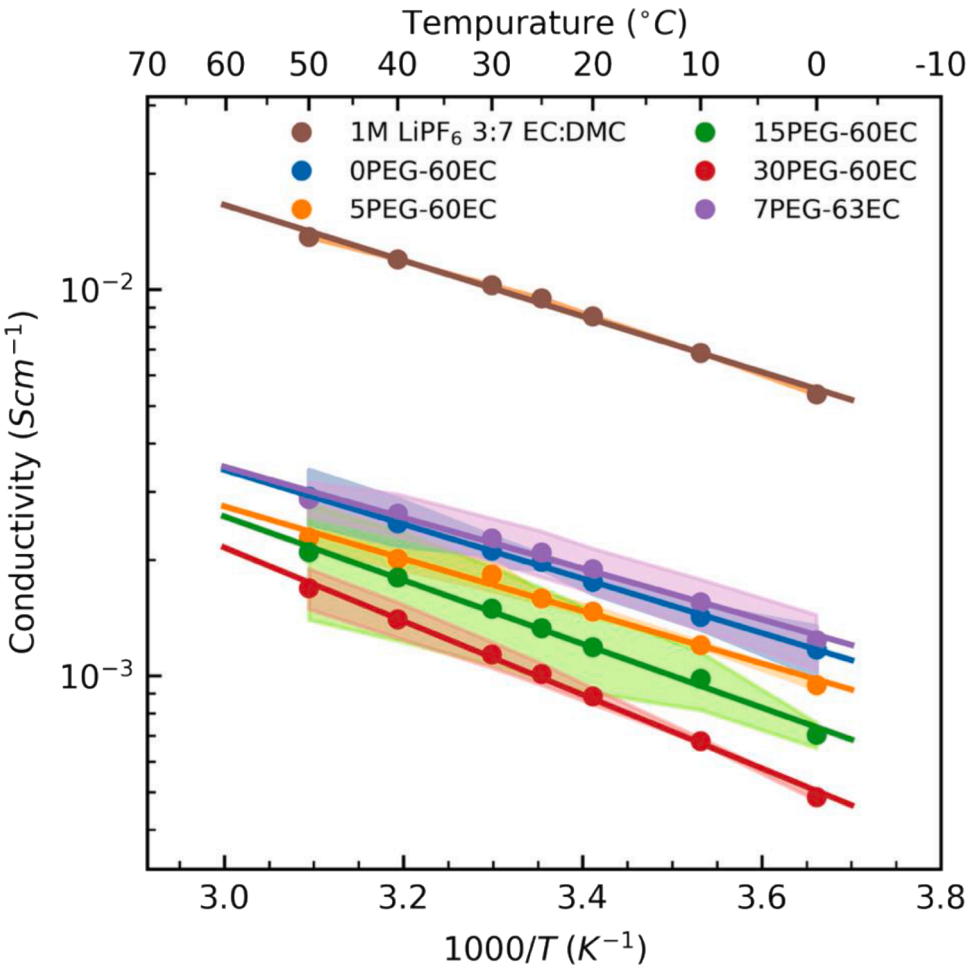

Fig. 4. Temperature dependence of the ionic conductivities of porous separators with comparison to liquid electrolyte (1M $LiPF_6$ in 3:7 v/v EC:DMC). Shaded backgrounds behind the data depict confidence in conductivity measurments. Linear regressions are plotted through the datasets to graphically indicate the activation energy.

morphology on transport relative to an homogeneous electrolyte solution and concisely communicates the expected ohmic overpotential contribution of the separator [75]. The equivalent N_M for each separator tested is in Table 1. A general requirement for LIB separators is a $N_M < 8$ [5]. Thus, the values for all PIPS separators herein are acceptable for use in LIBs, except 30PEG-60EC. 7PEG-63EC was measured to have the lowest N_M of 4.5, which is equal or superior to nearly all commercial separators previously reported in the literature. This includes (1) Celgard H2013, 2320, 2325, 2500, 3500, and C480, (2) PET membranes Separion S240P30 and Freidenberg FS-3001-30, and (3) two unnamed HDPE membranes as reported by Landesfield et al. [74], and (4) Celgard 2400, 2730, and (5) Solupor 14P01A, 3P07A and 10P05A as reported by Djian et al. [76].

To further examine the viability of all of these materials as LIB separator materials, lithium ion battery half cells with Li metal anodes and $LiNi_{0.5}Mn_{0.3}Co_{0.2}O_2$ (NMC532) cathodes were assembled using all five PIPS separators, as well as the commercial polypropylene benchmark, Celgard 2500. These cells were cycled at C/3 for 100 cycles between 3 V and 4.2 V vs. Li/Li^+. The capacity retention of all of these cells are shown in Fig. 5a. All of the cells cycled reversibly over 100 cycles, regardless of separator formulation, revealing the feasibility and physicochemical stability of the separators. Very slight variations in the discharge capacities of the cells are likely due to variations in separator thickness, conductivity, and random variations in cathode active material loading. However, all of the cells had good coulombic efficiency during cycling, indicating that no parasitic reactions occurred due to contamination within the separators or chemical incompatibility. The coulombic efficiency remained around 99% for most of the cycling, which is typical for cells using a lithium metal anode, due to the well-established instability of carbonate electrolytes on lithium metal [77, 78]. Minimal capacity fading was observed after 100 cycles, 0PEG-60EC retained 98.6% capacity, 5PEG-60EC retained 98.0%, 15PEG-60EC retained 96.4%, 30PEG-60EC retained 97.4%, and 7PEG-63EC retained 98.5%. In order to characterize the chemical stability of the optimized separator composition at more oxidizing potentials, 7PEG-63EC and Celgard 2500 were also cycled for 100 cycles between 3V and 4.4V vs Li/Li^+. The data collected is plotted in Fig. S4. Higher discharge capacities were achieved in both cells relative to the data in Fig. 5, due to the higher voltage accessing more lithium storage capacity. Both cells cycled stably over 100 cycles at nearly identical discharge capacities and coulombic efficiency, indicating that no parasitic reactions indicative of (electro)chemical instability of the separator were observed.

Corresponding voltage-discharge capacity curves for cycles 1, 50 and 100 are plotted in Fig. 5b,d. These show a typical discharge curve for a NMC532 cathode, gradually sloping before a fast drop in voltage around 3.6 V [79]. The slight variation in the profiles of samples is again the result of variations in separator thickness, ionic conductivity, and random deviations in cathode active material loading. The stability of these profiles after 100 cycles further demonstrates the success and stability in cycling LIB cells using the separators fabricated by PIPS, including those with short-PEG crosslinking functionalities. Rate tests

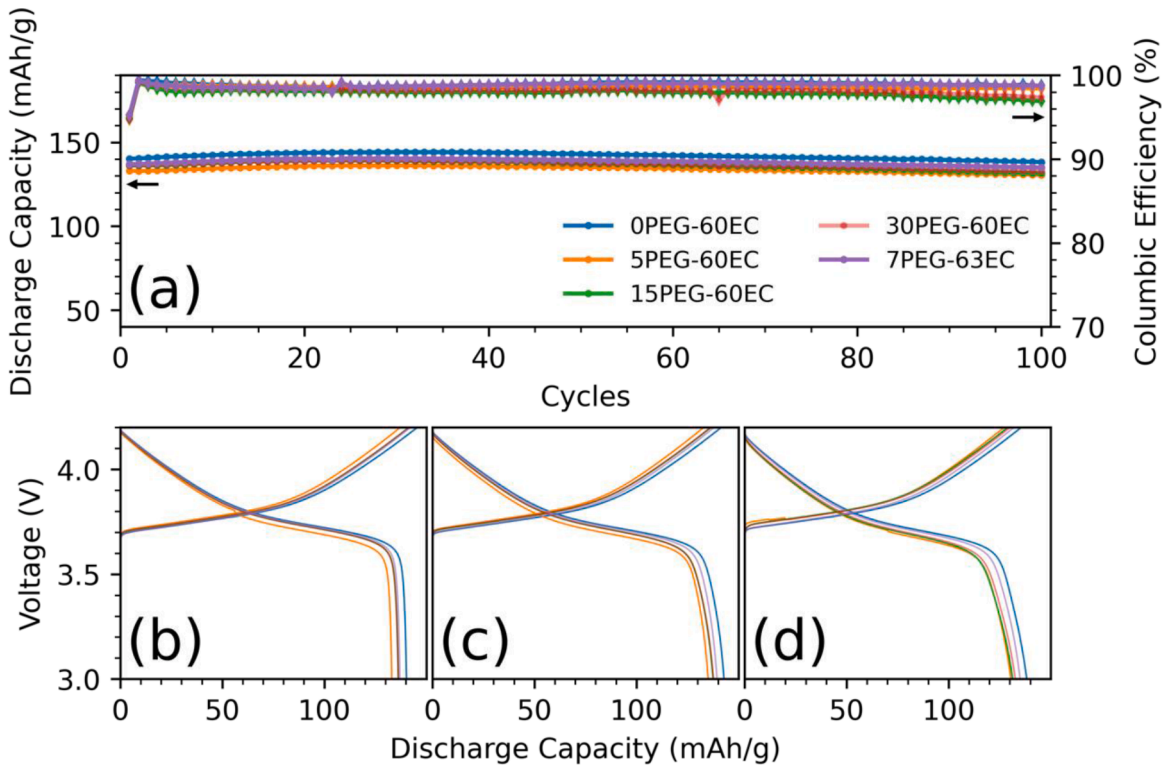

Fig. 5. Cycling data from NMC532/Lithium half-cells cycled at C/3 at 30 °C. 0PEG-60EC (28μm), 5PEG-60EC (38 μm), 15PEG-60EC (49 μm), 30PEG-60EC (41 μm) and 7PEG-63EC (21 μm) were incorporated into coin cells and the cycled. 1M $LiPF_6$ in 3:7 EC:DMC was used as electrolyte. (a) Discharge capacity (circles) and coulombic efficiency (diamonds) are plotted over 100 cycles. Voltage vs. discharge capacity profiles are plotted for the (b) 1st, (c) 50th and (d) 100th cycles.

were not performed on assembled coin cells. Based upon rate tests of the 0PEG-60EC formulation in prior work, it is expected that the PIPS separators will perform equally well [48]. Relative to Celgard 2500 the PIPS separators did not introduce a singificant overpotential at higher rates and comparable capacities are achieved. The discharge capacity of 0PEG-60EC dropped from 151.3 mAh g^{-1} at a C/10 rate to 123.9 mAh

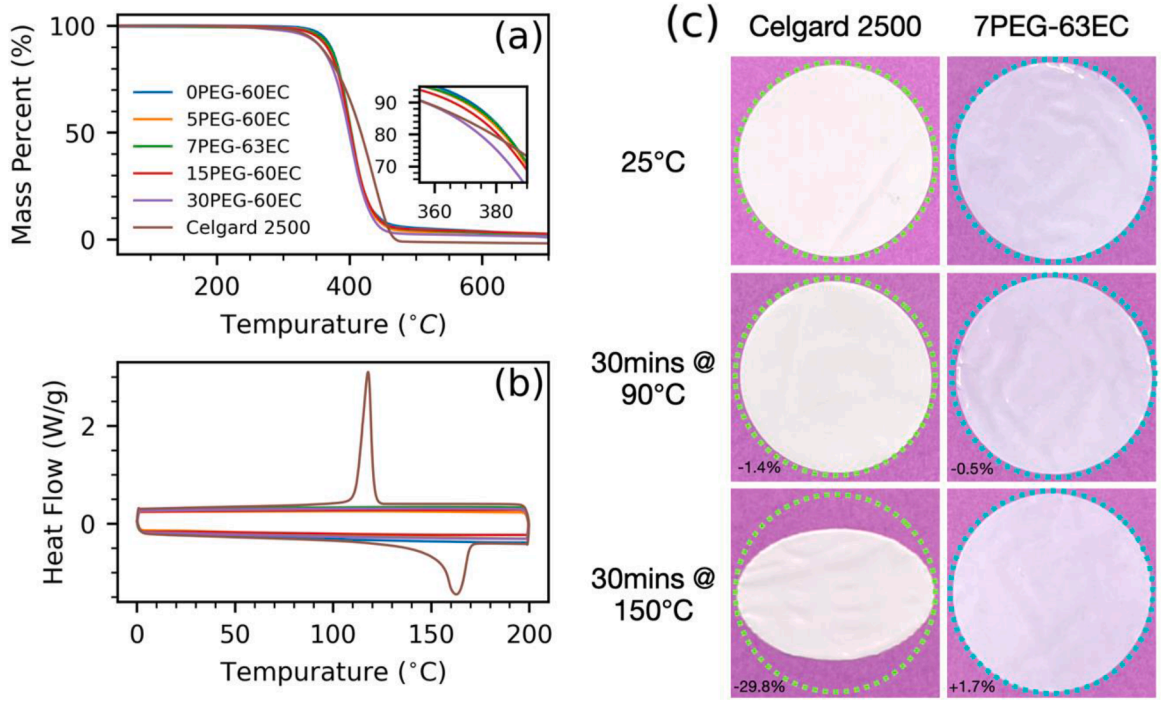

Fig. 6. Thermal characterization of separators. (a) Thermogravimentric analysis from 50 to 700°C at a ramp rate of 5 °C min^{-1}. (b) Differential scanning calorimetry from 0 to 200 °C at a ramp rate of 10 °C min^{-1} under a nitrogen gas purge. (c) Digital images of Celgard 2500 (25 μm) and 7PEG-63EC (19 μm) at room tempurature, and after heating for 30 min to 90 °C and 150 °C. The percentages in the bottom left of the images represent the change in separator area. The dotted outlines are references to the initial area of the samples.

g^{-1} at 3 C (18.1% drop) during the rate performance test. By comparison, the capacity of an identical cell incorporating Celgard 2500 was shown to drop from 143.5 mAh g^{-1} at C/10 to 121.0 mAh g^{-1} at 3 C (15.7%) [48].

The thermal and thermomechanical stability of the separators are also critical. Thermogravimetric analysis (TGA) in Fig. 6a reveals that all separator formulations have comparable thermal stability. When heated at a ramp rate of 5 °C min^{-1}, 0PEG-60EC, 5PEG-EC60 and 7PEG-EC63 were all stable to an onset temperature of 374 °C. At higher PEG contents, the thermal stability began to drop slightly, to an onset of 371 °C for 15PEG-60EC and 366 °C for 30PEG-60EC. This trend is due to the tendency of the ether bonds found in PEG chains to homolytically cleave at lower temperatures [80]. Approximately 5% (by mass) residual polymer remains after heating beyond 500 °C, which is attributed to β-scission of the ester functionalities leading to residual carbon char [81]. For comparison, the onset temperature of the commercial polypropylene separator was 375 °C. These thermal stabilities are all sufficient for use in a LIB, as other components degrade at lower temperatures. In particular, carbonate electrolytes begin to thermally decompose at 190 °C [82,83].

More salient to LIB applications, is the differential scanning calorimetry (DSC) data in Fig. 6b. This data reveals the absence of phase transitions in all PIPS formulations, which is attributed to the high degree of polymer crosslinking. This lack of phase transformation (melting) in the PIPS separators is expected to be a safety feature in large format (e.g. electric vehicle) lithium ion batteries. The polypropylene of Celgard 2500 melts at 160 °C, which is a safety hazard. In a thermal runaway scenario, once a cell reaches this melting temperature, the PP will lose structural integrity, leading to contact between electrodes. The resulting short circuit will generate heat, further accelerating the thermal runaway [16,84]. However, the melting of polyolefins has also been used as a design feature. Some LIBs incorporate what is known as a shutdown separator, which is typically a tri-layer membrane consisting of PP and PE in a PP/PE/PP arraignment. PE melts at a lower temperature than PP, at around 135 °C. In overcharge situations, once this temperature is reached, the PE layer melts, closing off the porosity of the separator, which sharply increases the ionic resistance and arrests lithium ion transport [12]. This is meant to shut off the current and stop the generation of heat. If this separator is able to shut down the thermal runaway before reaching the melting temperature PP, catastrophic cell failure may be prevented. While these types of separators have been extremely successful in small consumer electronics, there is evidence suggesting that the shutdown capabilities of such a separator is insufficient to halt lithium transport in large-scale, high-voltage applications such as batteries for electric vehicles and stationary storage [14,15]. Under these conditions, the PP still loses mechanical rigidity and contributes to thermal runaway, making polyolefin separators unsafe for these applications.

Despite not melting until 160 °C, the thermomechanical stability of PP is another critical safety concern at lower temperatures. Residual internal stresses are present in the PP due to the stretching steps in the manufacturing process of separators. As PP begins to soften well before its melting point, these internal stresses are relieved, leading to shrinkage. This thermal shrinkage phenomenon is a well-known safety issue in all polyolefin separators. To quantify thermal shrinkage, all PIPS separator formulations and Celgard 2500 were cut into circles, and their surface area was measured using a computer vision algorithm that detected the circular edge of the separator in a digital photograph and computed the area within that contour relative to a constant reference area. This analysis was performed on the separators first at room temperature, then after being held at elevated temperatures up to 150 °C for 30 min each. It was found that Celgard 2500 begins to shrink at temperatures as low as 90 °C, with a 1.4% reduction in area. At 150 °C, the Celgard 2500 shrank by 29.8%. None of the PIPS membranes were found to undergo significant thermal shrinkage at any temperature (up to 150 °C). Conversely, it was observed that these separators undergo a slight expansion at high temperatures, which increases with PEG content. This expansion is minimal and should not adversely affect cell performance. The results of the shrinkage test on Celgard 2500 and 7PEG-63EC are illustrated in Fig. 6c. The superior thermomechanical stability of the cross-linked PIPS separators is a beneficial feature for large-scale, high-voltage LIB applications. These separators could be used in tandem with proper external thermal management systems or combined with a polymer phase that does melt to form a more thermomechanically-stable shutdown separator. Both of these approaches would eliminate electrode short-circuiting as a driver of thermal runaway due to the excellent thermal stability of the PIPS separators.

Generally, the results of the experiments herein offer lessons and strategies for the further development of LIB separators. Opportunities for the fast and efficient development of new microporous separators to meet future technological demands were presented through co-polymerization and PIPS. Broad success of this co-polymer strategy is derived from the acrylate chemistry employed. It is possible to introduce nearly any chemical functionalities to the system, provided that it is linked to an acrylate functional group. Libraries of potential co-monomers are therefore available to explore formulations that may lead to next-generation battery separators. LIBs of the future will require such advanced separators with novel chemical multifunctionality to maximize the value of the component. Simultaneously, a pathway towards improving the mechanical properties of separators formed by PIPS was demonstrated, which may be necessary as other functional co-monomers can lead to weak and brittle polymer films, thus requiring the mechanical benefits afforded through the use of PEGDA. Furthermore, by using cross-linking monomers, polymer films that do not undergo thermal shrinkage or phase transitions are consistently prepared through PIPS, which offer significant safety benefits across all LIB applications.

4. Conclusion

In conclusion, the ability to tune the physical properties of microporous separators through the PIPS process has been demonstrated. By copolymerizing PEGDA with BDDA, increased conversion of the unsaturated vinyl functionalities is achieved. Both mechanical properties and pore morphologies possess a complex dependence with the PEGDA content in the polymer, with elastic modulus initially increasing with PEGDA content but then decreasing at higher PEGDA concentrations. The higher conversion is responsible for the increased elastic moduli at low PEGDA contents, but as PEGDA further increases, the crosslink density is reduced due to the PEG-400 chain interspersed between the reactive functionalities, leading to lower moduli but greater strain-to-failure. A similar complex trend in porosity is also observed. By optimizing the separator formulations for both elastic modulus and porosity, LIB separators were prepared that offer enhanced transport properties relative to commercial polyolefin separators yet possess sufficient mechanical properties for integration with existing roll-to-roll processing used in battery assembly. Using a PEGDA:BDDA ratio of 7:93 (by mass), and a porogen mass fraction of 63%, a microporous separator was prepared by one-step PIPS process with high porosity (41.3%), high ionic conductivity (2.09 ± 0.28 mS/cm), and an elastic modulus of 450 MPa. Moreover, due the highly crosslinked nature of the polymer matrix, the material does not melt or undergo thermal shrinkage, mitigating concerns over loss of cell structural integrity and electrode short-circuiting under high temperature abuse conditions.

All separators prepared by PIPS demonstrated excellent performance in a lithium ion battery half cells with $LiNi_{0.5}Mn_{0.3}Co_{0.2}O_2$ cathodes. All formulations demonstrated comparable performance to Celgard 2500. For example, the optimized 7PEG-63EC separator formulation demonstrated 98.5% capacity retention when cycled from 3.0 to 4.2 V vs. Li/Li^+ over 100 cycles – compared to 98.4% for Celgard. The advantage of the PIPS-based process is that new functionality can be incorporated into

the separators through modification of the precursor chemistry, transforming separators from passive to active components in lithium ion battery cells. Moreover, it can be designed as a one-step process eliminating the need for purification and other post-processing steps. Future studies can optimize the process to utilize electrolyte solutions, such as 1M $LiPF_6$ in EC:DMC, as porogens to further simplify separator fabrication and incorporation into the electrochemical cell. Additionally, copolymerization can imbue separators with additional functionality, such as acid-scavenging or polysulfide screening, to enable next-generation batteries though cost-effective, sustainable, scalable PIPS processing.

CRediT authorship contribution statement

Alexander J. Manly: Conceptualization, Investigation, Formal analysis, Writing – original draft. **Wyatt E. Tenhaeff:** Writing – review & editing, Supervision, Project administration, Funding acquisition.

Declaration of Competing Interest

The authors declare the following financial interests/personal relationships which may be considered as potential competing interests.

Data Availability

Data will be made available on request.

Funding

This material is based upon work supported by the National Science Foundation under Grant No. 1845805. This work was supported by the University of Rochester Materials Science Program. The NMC532 electrodes were produced at the U.S. Department of Energy's (DOE) CAMP (Cell Analysis, Modeling and Prototyping) Facility, Argonne National Laboratory. The CAMP Facility is fully supported by the DOE Vehicle Technologies Office (VTO).

Supplementary materials

Supplementary material associated with this article can be found, in the online version, at doi:10.1016/j.electacta.2022.140705.

References

[1] A. Kwade, W. Haselrieder, R. Leithoff, A. Modlinger, F. Dietrich, K. Droeder, Current status and challenges for automotive battery production technologies, Nat. Energy 3 (2018) 290–300, https://doi.org/10.1038/s41560-018-0130-3.
[2] J. Liu, Z. Bao, Y. Cui, E.J. Dufek, J.B. Goodenough, P. Khalifah, Q. Li, B.Y. Liaw, P. Liu, A. Manthiram, Y.S. Meng, V.R. Subramanian, M.F. Toney, V. V. Viswanathan, M.S. Whittingham, J. Xiao, W. Xu, J. Yang, X.Q. Yang, J.G. Zhang, Pathways for practical high-energy long-cycling lithium metal batteries, Nat. Energy 4 (2019) 180–186, https://doi.org/10.1038/s41560-019-0338-x.
[3] L. Zhang, X. Li, M. Yang, W. Chen, High-safety separators for lithium-ion batteries and sodium-ion batteries: advances and perspective, Energy Storage Mater. 41 (2021) 522–545, https://doi.org/10.1016/j.ensm.2021.06.033.
[4] Y. Li, L. Yu, W. Hu, X. Hu, Thermotolerant separators for safe lithium-ion batteries under extreme conditions, J. Mater. Chem. A 8 (2020) 20294–20317, https://doi.org/10.1039/D0TA07511F.
[5] P. Arora, Z. (John) Zhang, Battery separators, Chem. Rev. 104 (2004) 4419–4462, https://doi.org/10.1021/cr020738u.
[6] S.S. Zhang, A review on the separators of liquid electrolyte Li-ion batteries, J. Power Sources 164 (2007) 351–364, https://doi.org/10.1016/j.jpowsour.2006.10.065.
[7] V. Deimede, C. Elmasides, Separators for lithium-ion batteries: a review on the production processes and recent developments, Energy Technol. 3 (2015) 453–468, https://doi.org/10.1002/ente.201402215.
[8] C.M. Costa, Y.H. Lee, J.H. Kim, S.Y. Lee, S. Lanceros-Méndez, Recent advances on separator membranes for lithium-ion battery applications: From porous membranes to solid electrolytes, Energy Storage Mater. 22 (2019) 346–375, https://doi.org/10.1016/j.ensm.2019.07.024.
[9] M.F. Lagadec, R. Zahn, V. Wood, Characterization and performance evaluation of lithium-ion battery separators, Nat. Energy 4 (2019) 16–25, https://doi.org/10.1038/s41560-018-0295-9.
[10] H. Lee, Y. Meltem, O. Toprakci, K. Fu, X. Zhang, A review of recent developments in membrane separators for rechargeable lithium-ion batteries, Energy Environ. Sci. 7 (2014) 3857–3886.
[11] H. Zhang, M.Y. Zhou, C.E. Lin, B.K. Zhu, Progress in polymeric separators for lithium ion batteries, RSC Adv. 5 (2015) 89848–89860, https://doi.org/10.1039/C5RA14087K.
[12] K. Liu, Y. Liu, D. Lin, A. Pei, Y. Cui, Materials for lithium-ion battery safety, Sci. Adv. 4 (2018), https://doi.org/10.1126/sciadv.aas9820.
[13] P. Zhai, K. Liu, Z. Wang, L. Shi, S. Yuan, Multifunctional separators for high-performance lithium ion batteries, J. Power Sources 499 (2021), 229973, https://doi.org/10.1016/j.jpowsour.2021.229973.
[14] E.P. Roth, D.H. Doughty, D.L. Pile, Effects of separator breakdown on abuse response of 18650 Li-ion cells, J. Power Sources 174 (2007) 579–583, https://doi.org/10.1016/j.jpowsour.2007.06.163.
[15] C.J. Orendorff, T.N. Lambert, C.A. Chavez, M. Bencomo, K.R. Fenton, Polyester separators for lithium-ion cells: improving thermal stability and abuse tolerance, Adv. Energy Mater. 3 (2013) 314–320, https://doi.org/10.1002/aenm.201200292.
[16] L. Zhu, G. Ding, Q. Han, X. Yang, L. Xie, X. Cao, Review—recent developments in safety-enhancing separators for lithium-ion batteries, J. Electrochem. Soc. 168 (2021), 100524, https://doi.org/10.1149/1945-7111/ac2dca.
[17] H. Ma, J. Liu, H. Hua, L. Peng, X. Shen, X. Wang, P. Zhang, J. Zhao, Facile fabrication of functionalized separators for lithium-ion batteries with ionic conduction path modifications via the γ-ray co-irradiation grafting process, ACS Appl. Mater. Interfaces 13 (2021) 27663–27673, https://doi.org/10.1021/acsami.1c06460.
[18] L. Sheng, X. Xie, Z. Sun, M. Zhao, B. Gao, J. Pan, Y. Bai, S. Song, G. Liu, T. Wang, X. Huang, J. He, Role of separator surface polarity in boosting the lithium-ion transport property for a lithium-based battery, ACS Appl. Energy Mater. 4 (2021) 5212–5221, https://doi.org/10.1021/acsaem.1c00737.
[19] Z. Li, T. Cao, Y. Zhang, Y. Han, S. Xu, Z. Xu, Novel lithium ion battery separator based on hydroxymethyl functionalized poly(ether ether ketone), J. Membr. Sci. 540 (2017) 422–429, https://doi.org/10.1016/j.memsci.2017.06.045.
[20] R. Xu, L. Sheng, H. Gong, Y. Kong, Y. Yang, M. Li, Y. Bai, S. Song, G. Liu, T. Wang, X. Huang, J. He, High-performance Al_2O_3/PAALi composite separator prepared by water-based slurry for high-power density lithium-based battery, Adv. Energy Mater. 23 (2020), https://doi.org/10.1002/adem.202001009.
[21] Y. Song, L. Sheng, L. Wang, H. Xu, X. He, From separator to membrane: separators can function more in lithium ion batteries, Electrochem. Commun. 124 (2021), 106948, https://doi.org/10.1016/j.elecom.2021.106948.
[22] S. Ma, H. Lin, L. Yang, Q. Tong, F. Pan, J. Weng, S. Zheng, High thermal stability and low impedance polypropylene separator coated with aluminum phosphate, Electrochim. Acta 320 (2019), 134528, https://doi.org/10.1016/j.electacta.2019.07.039.
[23] Y. Xie, X. Chen, K. Han, X. Xiong, Natural halloysite nanotubes-coated polypropylene membrane as dual-function separator for highly safe Li-ion batteries with improved cycling and thermal stability, Electrochim. Acta 379 (2021), 138182, https://doi.org/10.1016/j.electacta.2021.138182.
[24] X. Huang, Separator technologies for lithium-ion batteries, J. Solid State Electrochem. 15 (2011) 649–662, https://doi.org/10.1007/s10008-010-1264-9.
[25] B. Yuan, K. Wen, D. Chen, Y. Liu, Y. Dong, C. Feng, Y. Han, J. Han, Y. Zhang, C. Xia, A. (Xueliang) Sun, W. He, Composite separators for robust high rate lithium ion batteries, Adv. Funct. Mater. 31 (2021), 2101420, https://doi.org/10.1002/adfm.202101420.
[26] M.R. Asghar, M.T. Anwar, A. Naveed, J. Zhang, A review on inorganic nanoparticles modified composite membranes for lithium-ion batteries: recent progress and prospects, Membranes 9 (2019) 78, https://doi.org/10.3390/membranes9070078.
[27] N. Wei, J. Hu, M. Zhang, J. He, P. Ni, Cross-linked porous polymer separator using vinyl-modified aluminum oxide nanoparticles as cross-linker for lithium-ion batteries, Electrochim. Acta 307 (2019) 495–502, https://doi.org/10.1016/j.electacta.2019.04.010.
[28] H. Li, B. Zhang, W. Liu, B. Lin, Q. Ou, H. Wang, M. Fang, D. Liu, S. Neelakandan, L. Wang, Effects of an electrospun fluorinated poly(ether ether ketone) separator on the enhanced safety and electrochemical properties of lithium ion batteries, Electrochim. Acta 290 (2018) 150–164, https://doi.org/10.1016/j.electacta.2018.08.075.
[29] L. Wang, N. Deng, J. Ju, G. Wang, B. Cheng, W. Kang, A novel core-shell structured poly-m-phenyleneisophthalamide@polyvinylidene fluoride nanofiber membrane for lithium ion batteries with high-safety and stable electrochemical performance, Electrochim. Acta 300 (2019) 263–273, https://doi.org/10.1016/j.electacta.2019.01.115.
[30] W. Luo, S. Cheng, M. Wu, X. Zhang, D. Yang, X. Rui, A review of advanced separators for rechargeable batteries, J. Power Sources 509 (2021), https://doi.org/10.1016/j.jpowsour.2021.230372.
[31] W. Zhang, Z. Tu, J. Qian, S. Choudhury, L.A. Archer, Y. Lu, Design principles of functional polymer separators for high-energy, metal-based batteries, Small 14 (2018), 1703001, https://doi.org/10.1002/smll.201703001.
[32] Y. Pang, Y. Cao, Y. Chu, M. Liu, K. Snyder, D. MacKenzie, C. Cao, Additive manufacturing of batteries, Adv. Funct. Mater. 30 (2020), 1906244, https://doi.org/10.1002/adfm.201906244.
[33] A. Banerjee, B. Ziv, Y. Shilina, S. Luski, D. Aurbach, I.C. Halalay, Improving stability of li-ion batteries by means of transition metal ions trapping separators,

J. Electrochem. Soc. 163 (2016) A1083–A1094, https://doi.org/10.1149/2.0081607jes.
[34] Y. Shilina, S. Maddukuri, A. Banerjee, B. Ziv, S. Luski, D. Aurbach, I.C. Halalay, LNMO-graphite cells performance enhancement by the use of acid scavenging separators, ChemElectroChem 6 (2019) 3690–3698, https://doi.org/10.1002/celc.201900907.
[35] A. Banerjee, B. Ziv, Y. Shilina, J.M. Ziegelbauer, H. Liu, K.J. Harris, G. Botton, G. R. Goward, S. Luski, D. Aurbach, I.C. Halalay, Review—multifunctional separators: a promising approach for improving the durability and performance of li-ion batteries, J. Electrochem. Soc. 166 (2019) A5369–A5377, https://doi.org/10.1149/2.0561903jes.
[36] A. Banerjee, B. Ziv, S. Luski, D. Aurbach, I.C. Halalay, Increasing the durability of Li-ion batteries by means of manganese ion trapping materials with nitrogen functionalities, J. Power Sources 341 (2017) 457–465, https://doi.org/10.1016/j.jpowsour.2016.12.036.
[37] A. Banerjee, B. Ziv, Y. Shilina, S. Luski, D. Aurbach, I.C. Halalay, Acid-scavenging separators: a novel route for improving li-ion batteries' durability, ACS Energy Lett. 2 (2017) 2388–2393, https://doi.org/10.1021/acsenergylett.7b00763.
[38] A. Banerjee, B. Ziv, Y. Shilina, S. Luski, I.C. Halalay, D. Aurbach, Multifunctional manganese ions trapping and hydrofluoric acid scavenging separator for lithium ion batteries based on poly(ethylene-alternate-maleic acid) dilithium salt, Adv. Energy Mater. 7 (2017) 1601556, https://doi.org/10.1002/aenm.201601556.
[39] F.A. Susai, H. Sclar, Y. Shilina, T. Rao Penki, R. Raman, S. Maddukuri, S. Maiti, I. C. Halalay, S. Luski, B. Markovsky, D. Aurbach, Horizons for li-ion batteries relevant to electro-mobility: high-specific-energy cathodes and chemically active separators, J. Adv. Mater. 30 (2018), https://doi.org/10.1002/adma.201801348.
[40] C. Ma, Y. Feng, X. Liu, Y. Yang, L. Zhou, L. Chen, C. Yan, W. Wei, Dual-engineered separator for highly robust, all-climate lithium-sulfur batteries, Energy Storage Mater. 32 (2020) 46–54, https://doi.org/10.1016/j.ensm.2020.07.034.
[41] C. Deng, Z. Wang, L. Feng, S. Wang, J. Yu, Electrocatalysis of sulfur and polysulfides in Li–S batteries, J. Mater. Chem. A 8 (2020) 19704–19728, https://doi.org/10.1039/D0TA05964A.
[42] C. Deng, Z. Wang, S. Wang, J. Yu, Inhibition of polysulfide diffusion in lithium–sulfur batteries: mechanism and improvement strategies, J. Mater. Chem. A 7 (2019) 12381–12413, https://doi.org/10.1039/C9TA00535H.
[43] Y. Feng, G. Wang, W. Kang, N. Deng, B. Cheng, Taming polysulfides and facilitating lithium-ion migration: novel electrospinning MOFs@PVDF-based composite separator with spiderweb-like structure for Li-S batteries, Electrochim. Acta 365 (2021), 137344, https://doi.org/10.1016/j.electacta.2020.137344.
[44] B. Yu, Y. Fan, S. Mateti, D. Kim, C. Zhao, S. Lu, X. Liu, Q. Rong, T. Tao, K. K. Tanwar, X. Tan, S.C. Smith, Y.I. Chen, An ultra-long-life flexible lithium–sulfur battery with lithium cloth anode and polysulfone-functionalized separator, ACS Nano 15 (2021) 1358–1369, https://doi.org/10.1021/acsnano.0c08627.
[45] C.H. Chang, S.H. Chung, P. Han, A. Manthiram, Oligoanilines as a suppressor of polysulfide shuttling in lithium–sulfur batteries, Mater. Horiz. 4 (2017) 908–914, https://doi.org/10.1039/C7MH00510E.
[46] L.M. Schneider, N. Ihrner, D. Zenkert, M. Johansson, Bicontinuous electrolytes via thermally initiated polymerization for structural lithium ion batteries, ACS Appl. Energy Mater. 2 (2019) 4362–4369, https://doi.org/10.1021/acsaem.9b00563.
[47] N. Ihrner, W. Johannisson, F. Sieland, D. Zenkert, M. Johansson, Structural lithium ion battery electrolytes *via* reaction induced phase-separation, J. Mater. Chem. A 5 (2017) 25652–25659, https://doi.org/10.1039/C7TA04684G.
[48] A.J. Manly, W.E. Tenhaeff, One-step fabrication of robust lithium ion battery separators by polymerization-induced phase separation, J. Mater. Chem. A (2022), https://doi.org/10.1039/D1TA10730E.
[49] Z. Xue, L. Hu, K. Amine, Z. Zhang, High-speed fabrication of lithium-ion battery electrodes by UV-curing, Energy Technol. 3 (2015) 469–475, https://doi.org/10.1002/ente.201402210.
[50] Z. Luo, Y. Xu, C.R. Gong, Y.Q. Zheng, Z.X. Zhou, L.M. Yu, An ultraviolet curable silicon/graphite electrode binder for long-cycling lithium ion batteries, J. Power Sources 485 (2021), 229348, https://doi.org/10.1016/j.jpowsour.2020.229348.
[51] J.P. Fouassier, Photoinitiation, Photopolymerization, and Photocuring: Fundamentals and Applications, Hanser Distributed by Hanser/Gardner Publications, Munich, 1995.
[52] H. Li, X.T. Ma, J.L. Shi, Z.K. Yao, B.K. Zhu, L.P. Zhu, Preparation and properties of poly(ethylene oxide) gel filled polypropylene separators and their corresponding gel polymer electrolytes for Li-ion batteries, Electrochim. Acta 56 (2011) 2641–2647, https://doi.org/10.1016/j.electacta.2010.12.010.
[53] Y. Jiang, X. Yan, Z. Ma, P. Mei, W. Xiao, Q. You, Y. Zhang, Development of the PEO based solid polymer electrolytes for all-solid state lithium ion batteries, Polymers 10 (2018) 1237, https://doi.org/10.3390/polym10111237.
[54] Z. Li, Y. Zhao, W.E. Tenhaeff, Determining the absolute anodic stability threshold of polymer electrolytes: a capacity-based electrochemical method, Chem. Mater. 33 (2021) 1927–1934, https://doi.org/10.1021/acs.chemmater.0c04248.
[55] G. Bradski, The OpenCV library, Dr, Dobb's Journal of Software Tools 120 (2000) 122–125.
[56] B.R. Long, S.G. Rinaldo, K.G. Gallagher, D.W. Dees, S.E. Trask, B.J. Polzin, A. N. Jansen, D.P. Abraham, I. Bloom, J. Bareño, J.R. Croy, Enabling high-energy, high-voltage lithium-ion cells: standardization of coin-cell assembly, electrochemical testing, and evaluation of full cells, J. Electrochem. Soc. 163 (2016) A2999–A3009, https://doi.org/10.1149/2.0691614jes.
[57] A. Udagawa, F. Sakurai, T. Takahashi, *In situ* study of photopolymerization by fourier transform infrared spectroscopy, J. Appl. Polym. Sci. 42 (1991) 1861–1867, https://doi.org/10.1002/app.1991.070420707.
[58] E. Khairuddin, S.B. Pramono, V. Utomo, A. Wulandari, W Zahrotul, F. Clegg, FTIR studies on the effect of concentration of polyethylene glycol on polimerization of Shellac, J. Phys. Conf. Ser. 776 (2016), 012053, https://doi.org/10.1088/1742-6596/776/1/012053.
[59] W.R. Feairheller, J.E. Katon, The vibrational spectra of acrylic acid and sodium acrylate, Spectrochim. Acta A Mol. Spectrosc. 23 (1967) 2225–2232, https://doi.org/10.1016/0584-8539(67)80114-4.
[60] C. Decker, K. Moussa, Real-time kinetic study of laser-induced polymerization, Macromolecules 22 (1989) 4455–4462, https://doi.org/10.1021/ma00202a013.
[61] R.A. Scott, N.A. Peppas, Kinetics of copolymerization of PEG-containing multiacrylates with acrylic acid, Macromolecules 32 (1999) 6149–6158, https://doi.org/10.1021/ma9806110.
[62] C. Ishino, K. Okumura, Wetting transitions on textured hydrophilic surfaces, Eur. Phys. J. E 25 (2008) 415–424, https://doi.org/10.1140/epje/i2007-10308-y.
[63] Y. Liu, Polymerization-induced phase separation and resulting thermomechanical properties of thermosetting/reactive nonlinear polymer blends: a review, J. Appl. Polym. Sci. 127 (2013) 3279–3292, https://doi.org/10.1002/app.38721.
[64] R. Bella, P. Cassagnau, F. Fenouillot, Reaction and morphology development influenced by diffusion in a thermoplastic/thermoset blend, Macromol. Symp. 233 (2006) 59–65, https://doi.org/10.1002/masy.200690029.
[65] N. Boyard, M. Vayer, C. Sinturel, S. Seifert, R. Erre, Investigation of phase separation mechanisms of thermoset polymer blends by time-resolved SAXS, Eur. Polym. J. 41 (2005) 1333–1341, https://doi.org/10.1016/j.eurpolymj.2005.01.005.
[66] N. Boyard, M. Vayer, Ch. Sinturel, R. Erre, Phase-separation mechanism and corresponding final morphologies of thermoset blends based on unsaturated polyester and low-molar-weight saturated polyester, J. Appl. Polym. Sci. 95 (2005) 1459–1472, https://doi.org/10.1002/app.21392.
[67] J.Y. Song, Y.Y. Wang, C.C. Wan, Review of gel-type polymer electrolytes for lithium-ion batteries, J. Power Sources 77 (1999) 183–197, https://doi.org/10.1016/S0378-7753(98)00193-1.
[68] M.K. Song, J.Y. Cho, B.W. Cho, H.W. Rhee, Characterization of UV-cured gel polymer electrolytes for rechargeable lithium batteries, J. Power Sources 110 (2002) 209–215, https://doi.org/10.1016/S0378-7753(02)00258-6.
[69] M.K. Song, Y.T. Kim, J.Y. Cho, B.W. Cho, B.N. Popov, H.W. Rhee, Composite polymer electrolytes reinforced by non-woven fabrics, J. Power Sources 125 (2004) 10–16, https://doi.org/10.1016/S0378-7753(03)00826-7.
[70] C.M. Yang, H.S. Kim, B.K. Na, K.S. Kum, B.W. Cho, Gel-type polymer electrolytes with different types of ceramic fillers and lithium salts for lithium-ion polymer batteries, J. Power Sources 156 (2006) 574–580, https://doi.org/10.1016/j.jpowsour.2005.06.018.
[71] H. Duan, M. Fan, W. Chen, J. Li, P. Wang, W. Wang, J. Shi, Y. Yin, L. Wan, Y. Guo, Extended electrochemical window of solid electrolytes via heterogeneous multilayered structure for high-voltage lithium metal batteries, Adv. Mater. 31 (2019), 1807789, https://doi.org/10.1002/adma.201807789.
[72] A.M. Stephan, Review on gel polymer electrolytes for lithium batteries, Eur. Polym. J. 42 (2006) 21–42, https://doi.org/10.1016/j.eurpolymj.2005.09.017.
[73] K.M. Abraham, Directions in secondary lithium battery research and development, Electrochim. Acta 38 (1993) 1233–1248, https://doi.org/10.1016/0013-4686(93)80054-4.
[74] J. Landesfeind, J. Hattendorff, A. Ehrl, W.A. Wall, H.A. Gasteiger, Tortuosity determination of battery electrodes and separators by impedance spectroscopy, J. Electrochem. Soc. 163 (2016) A1373–A1387, https://doi.org/10.1149/2.1141607jes.
[75] R. Raccichini, L. Furness, J.W. Dibden, J.R. Owen, N. García-Araez, Impedance characterization of the transport properties of electrolytes contained within porous electrodes and separators useful for Li-S batteries, J. Electrochem. Soc. 165 (2018) A2741–A2749, https://doi.org/10.1149/2.0631811jes.
[76] D. Djian, F. Alloin, S. Martinet, H. Lignier, J.Y. Sanchez, Lithium-ion batteries with high charge rate capacity: influence of the porous separator, J. Power Sources 172 (2007) 416–421, https://doi.org/10.1016/j.jpowsour.2007.07.018.
[77] W. Xu, J. Wang, F. Ding, X. Chen, E. Nasybulin, Y. Zhang, J.G. Zhang, Lithium metal anodes for rechargeable batteries, Energy Environ. Sci. 7 (2014) 513–537, https://doi.org/10.1039/C3EE40795K.
[78] J. Xiao, Q. Li, Y. Bi, M. Cai, B. Dunn, T. Glossmann, J. Liu, T. Osaka, R. Sugiura, B. Wu, J. Yang, J.G. Zhang, M.S. Whittingham, Understanding and applying coulombic efficiency in lithium metal batteries, Nat. Energy 5 (2020) 561–568, https://doi.org/10.1038/s41560-020-0648-z.
[79] S.J. Kwon, S.E. Lee, J.H. Lim, J. Choi, J. Kim, Performance and life degradation characteristics analysis of NCM LIB for BESS, Electronics 7 (2018), https://doi.org/10.3390/electronics7120406.
[80] R.P. Lattimer, Mass spectral analysis of low-temperature pyrolysis products from poly(ethylene glycol), J. Anal. Appl. Pyrolysis 56 (2000) 61–78, https://doi.org/10.1016/S0165-2370(00)00074-7.
[81] I.C. McNeill, M.H. Mohammed, A comparison of the thermal degradation behaviour of ethylene-ethyl acrylate copolymer, low density polyethylene and poly (ethyl acrylate), Polym. Degrad. Stab. 48 (1995) 175–187, https://doi.org/10.1016/0141-3910(95)00030-P.
[82] G.G. Botte, R.E. White, Z. Zhang, Thermal stability of LiPF6–EC:EMC electrolyte for lithium ion batteries, J. Power Sources 97–98 (2001) 570–575, https://doi.org/10.1016/S0378-7753(01)00746-7.
[83] B. Ravdel, K.M. Abraham, R. Gitzendanner, J. DiCarlo, B. Lucht, C. Campion, Thermal stability of lithium-ion battery electrolytes, J. Power Sources 119–121 (2003) 805–810, https://doi.org/10.1016/S0378-7753(03)00257-X.
[84] M. Yuan, K. Liu, Rational design on separators and liquid electrolytes for safer lithium-ion batteries, J. Energy Chem. 43 (2020) 58–70, https://doi.org/10.1016/j.jechem.2019.08.008.